Noise, multistability, and delayed recurrent loops

Jennifer Foss,[1] Frank Moss,[2] and John Milton[1]
[1]*Department of Neurology and Committee on Neurobiology, The University of Chicago, Chicago, Illinois 60637*
[2]*Department of Physics, University of Missouri at St. Louis, St. Louis, Missouri 63121*
(Received 9 August 1996)

The multistability that arises in delayed feedback control mechanisms has applications for dynamic short term memory storage. Here we investigate the effects of multiplicative, Gaussian-distributed white noise on an integrate-and-fire model of a recurrent inhibitory neural loop: when the neuron fires an inhibitory pulse decreases the membrane potential by an amount Δ at time τ later. For appropriate choices of τ and Δ, multistability occurs in the form of qualitatively different neuron firing patterns. In the absence of noise, the number and nature of the coexistent attractors can be precisely determined. When noise is added to Δ, noise-induced transitions occur between the attractors. The mechanism for these transitions is characterized and it is shown that the rate of transitions has a nonexponential dependence on the noise variance. An electronic circuit is constructed to assess the impact of noise on memory storage. [S1063-651X(97)08404-3]

PACS number(s): 87.10.+e, 05.40.+j, 02.30.Ks

I. INTRODUCTION

A multistable dynamical system is one in which multiple attractors coexist. Each attractor pulls in trajectories that fall within a certain basin of attraction. Multiple limit cycle attractors have been observed in models of neurons [1] and neural recurrent loops [2] and have been observed experimentally in excitable cells [3] and in neural circuits constructed from invertebrate neurons [4]. More generically, multiple limit cycle attractors arise in time-delayed feedback mechanisms; an example is the first-order delay differential equation (DDE)

$$\dot{x}+\alpha x=f(x(t-\tau)), \tag{1}$$

where α is a positive rate constant [5,6]. Previous studies have suggested that multistability occurs when the time delay τ is longer than the intrinsic time scale of the control mechanism, i.e., $\tau>\alpha^{-1}$, and the feedback f is nonmonotonic [6]. This has been demonstrated in experiments involving time-delayed electronic circuits ([7], and this communication) and optical dye lasers [8]. When (1) is replaced by a second-order DDE multistability arises even in the case where f is monotonic, negative feedback [9]. Here we consider a multistable dynamical system in which the attractors are of limit cycle type.

Multistability has been emphasized as a mechanism for dynamic memory storage [2,6,8]; each attractor is identified with a different memory. In neural networks the existence of multiple fixed point (or limit cycle) attractors lies at the basis of proposed mechanisms for associative content-addressable memory [10]. However, stochastic perturbations (''noise'') place important limitations on the ability of multistable systems to store memory [1]. For example, noise can cause switches between basins of attraction. Noise-induced transitions in bistable systems have been studied extensively [11,12], particularly in the context of the detection of weak periodic signals [13]. However, little work has appeared on the effects of noise on systems in which retarded variables play a major role [14]. A fundamental difficulty is that in order to solve a DDE it is necessary to specify an initial function $\phi(s)$, $s\in[-\tau,0]$. Thus it is necessary to study the effects of noise in the setting of a functional space.

Here we study the noise-induced transitions that occur between coexistent limit cycle attractors in an integrate-and-fire model for a recurrent inhibitory neural loop [Fig. 1(a)] [2]. In Sec. II we determine the number of attractors and their properties for this model in the absence of noise. In Sec. III we characterize the mechanism for noise-induced transitions between attractors. Finally, in Sec. IV we study the

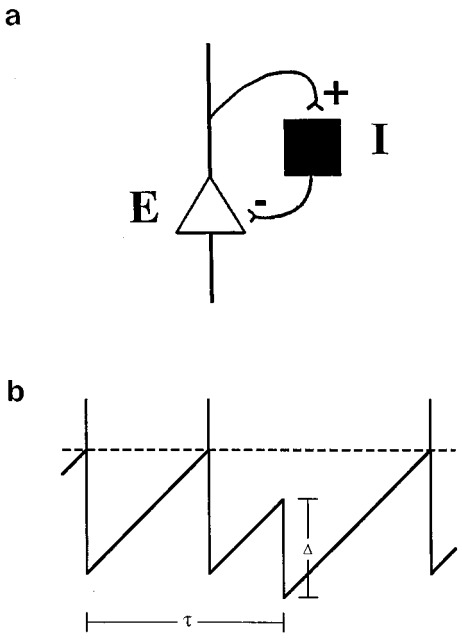

FIG. 1. (a) Schematic diagram of a neural recurrent inhibitory feedback loop. Neuron E makes an excitatory synapse onto the inhibitory interneuron I, which in turn makes an inhibitory synapse back onto E. (b) The time course of the membrane potential v for the integrate-and-fire neuron E under time-delayed inhibitory feedback. The dashed line indicates the threshold θ. (See text for details.)

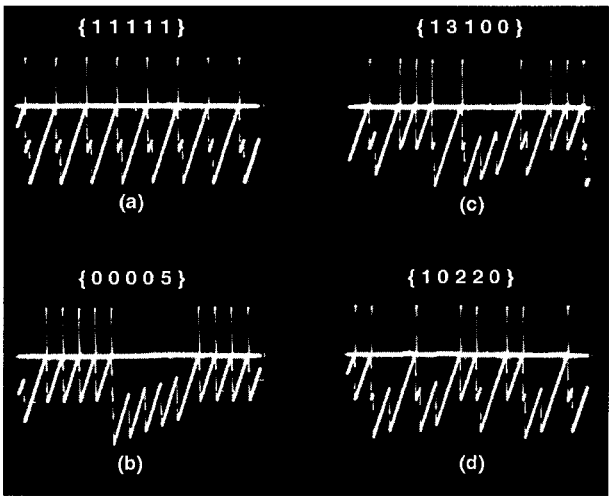

FIG. 2. The four distinct attractors (a)–(d), which coexist when $\tau=4.01$ and $\Delta=0.89$ for the circuit model (Appendix). The same attractors are found analytically (Sec. II). The notation {} describes the periodic sequences by the number of inhibitory pulses in each interspike interval.

effects of noise on the memory storage capabilities of an electronic circuit analog of the integrate-and-fire delayed recurrent loop.

II. MODEL

An integrate-and-fire model for a recurrent inhibitory loop is presented in Fig. 1(b). The membrane potential v of the neuron increases linearly at a rate A until it reaches the firing threshold θ. When $v=\theta$, the neuron fires and v is reset to its resting membrane potential v_0. The firing of the neuron excites the inhibitory interneuron such that at a time τ later the membrane potential of the excitatory neuron is decreased by an amount Δ. In the absence of recurrent inhibition the period $T=\theta/A$.

For ease of analysis, we have nondimensionalized the system so that the rate of rise of the membrane potential and the threshold are 1, while the resting potential is taken to be 0, giving the neuron a firing period of 1. We shall use the same variable names to denote the new dimensionless versions. Now the temporal pattern of the spikes generated by E depends on two parameters: τ and Δ. The special case $\tau=q$, q a positive integer, has been briefly considered previously [15]. Here we consider all positive τ.

When $\tau<1$, the RI (recurrent inhibition) model produces only a regular periodic firing pattern. Each excitatory spike produced is followed by an inhibitory pulse at time τ later. The inhibitory pulse decreases v by an amount Δ and hence prolongs the period by an amount Δ. Thus all solutions are periodic with period $1+\Delta$. This case has been explored extensively in the context of fixed delay stimulation of cardiac and respiratory oscillators [16]. We do not consider this case further.

Multistability arises when $\tau>1$ [2]. This complex behavior becomes possible since the inhibitory pulses are not necessarily the result of the immediately preceding excitatory spike (Fig. 2). For example, four different attractors occur

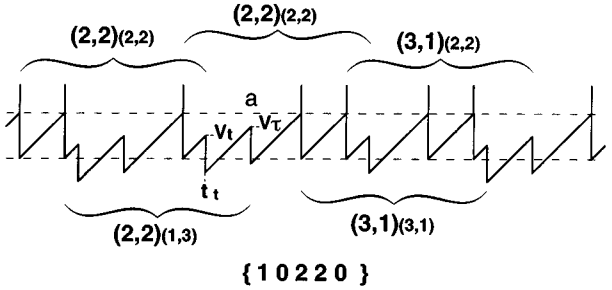

FIG. 3. Representation of the pattern {10220} in intervals of length τ, which are denoted by the brackets above and below. See text for discussion.

when $\tau=4.1$ and $\Delta=0.8$ (Fig. 2). Here we demonstrate that all attractors in this model are periodic and can be completely described. We introduce the following notation: A periodic spike train consisting of j interspike intervals (ISI) is completely described by the notation $\{n_1,n_2,\ldots,n_j\}$, where n_i is the number of times that the inhibitory neuron fires in the ith interval. Necessarily, $j=\sum_{i=1}^{j}n_i$, i.e., some of the n_i may be zero.

In order to determine the general solution of this model, consider the spike pattern shown in Fig. 3. We construct the time series in intervals of length τ and identify the beginning of this interval with the occurrence of a spike. The time between two consecutive excitatory spikes is $1+p\Delta$, p a non-negative integer, and the time between two consecutive inhibitory pulses that are not separated by a spike is one [17]. Following each spike an inhibitory pulse occurs τ later. For example, consider $t=a$ in Fig. 3. The voltage at the time the inhibitory pulse occurs, v_τ, is (Fig. 3)

$$v_\tau=v_t+m_v-n_v\Delta, \tag{2}$$

where m_v, n_v are non-negative integers and v_t is the voltage at the time t_t, the first inhibitory pulse that occurs following the last spike, $0<v_t<1$, and it follows that $0<v_\tau<1$. In Fig. 3, when $t=a$, $v_\tau=v_t+1-\Delta$.

The time t_t can be uniquely determined by

$$\tau=t_t+m_\tau+n_\tau\Delta, \tag{3}$$

where m_τ,n_τ are positive integers and $0<t_t<1$. At $t=a$ we have $t_t=\tau-2-2\Delta$.

Since $v_t=t_t$ (these are dimensionless numbers and $A=1$) we can substitute Eq. (2) into (3) to obtain

$$\tau=v_\tau+(m_\tau-m_v)+(n_\tau+n_v)\Delta=v_\tau+M+N\Delta. \tag{4}$$

At $t=a$ we have $v_\tau=\tau-1-3\Delta$.

Equations (3) and (4) are of the same general form, i.e.,

$$\tau=m+n\Delta+x, \tag{5}$$

where m,n are positive integers such that $0\leqslant m\leqslant\tau$, $0\leqslant n\leqslant\tau/\Delta$, and $0<x<1$. For τ,Δ fixed, the total number of (m,n) pairs that satisfy Eq. (5) is $\lceil\tau/\Delta\rceil$, where the notation $\lceil\rceil$ denotes the smallest integer greater than τ/Δ.

Thus the solution of the RI model is constructed from segments of length τ, each of which is described by the double pair of non-negative integers, denoted $(m_\tau,n_\tau)_{(M,N)}$, where (m_τ,n_τ) and (M,N) simultaneously satisfy, respectively, Eqs. (3) and (4) (Fig. 3) subject to the

conditions that $m_\tau > m_v$ and $m_v = n_v$ [17]. For each $(m_\tau, n_\tau)_{(M,N)}$ the total number of allowable segments of length τ (i.e., $M < m_\tau$, $N > n_\tau$), P, is

$$P = \begin{cases} \prod_{i=1}^{M-1} \frac{n_\tau + i}{i} & \text{if } M > 1 \\ 1 & \text{if } M = 1 \\ 1 & \text{if } M = n_\tau = 0 \\ 0 & \text{if } M = 0, n_\tau \neq 0 \end{cases}$$

For example, when $\tau = 4.1$ and $\Delta = 0.8$, the possible (m,n) pairs satisfying Eq. (11) are (4,0), (3,1), (2,2), (1,3), and (0,4) corresponding to 16 distinct segments $(m_\tau, n_\tau)_{(M,N)}$.

Since the number of $(m_\tau, n_\tau)_{(M,N)}$ segments is finite for fixed τ, Δ, it follows that all solutions of the RI model are periodic. Moreover, since there is a one-to-one relationship between excitatory spikes and inhibitory pulses, and since each inhibitory pulse prolongs the period by Δ, the period of these solutions is $S(1+\Delta)$, where S is a positive integer equal to the number of excitatory spikes per period. The mean interspike interval is therefore $(1+\Delta)$.

The solution of the RI model can be uniquely written as a sequence of $(m_\tau, n_\tau)_{(M,N)}$ segments; which segment is used depends on the previous segment (Fig. 3). In general, not all of the possible segments are incorporated into one of the steady state solutions. However, in the case of $\tau = 4.1$, $\Delta = 0.8$, all of the possible segments are utilized. There is one periodic solution described by $\{(2,2)_{(2,2)}\}$ [Fig. 2(a)], and three different periodic solutions corresponding, respectively, to a bursting pattern, $\{(4,0)_{(4,0)}, (4,0)_{(3,1)}, (4,0)_{(2,2)}, (4,0)_{(1,3)}, (4,0)_{(0,4)}\}$ [Fig. 2(b)], and two more complex patterns: $\{(3,1)_{(3,1)}, (3,1)_{(2,2)}, (2,2)_{(2,2)}, (2,2)_{(1,3)}, (2,2)_{(2,2)}\}$ [Fig. 2(c)] and $\{(3,1)_{(3,1)}, (3,1)_{(2,2)}, (3,1)_{(1,3)}, (1,3)_{(1,3)}, (3,1)_{(3,1)}$ [Fig. 2(d)].

Once the solutions are known we can readily determine all values of τ and Δ for which each solution exists. Regular spiking patterns [Fig. 2(a)], i.e., $\{1\}_j \equiv \{1_1, 1_2, \ldots, 1_j\}$ occur when [18]

$$(j-1)(1+\Delta) < \tau < (j-1)(1+\Delta) + 1$$

and bursting patterns [Fig. 2(b)], i.e., $\{0,j\}_j \equiv \{0,0,\ldots,0,j\}$ when

$$j - 1 < \tau < \Delta(j-1) + 1.$$

The more complex patterns shown in Figs. 2(c) and 2(d), respectively, i.e.,

$$\{13100\}_k \equiv \{R_1,\ R_2,\ R_3, \ldots,\ R_k\},$$

$$\{10220\}_k \equiv \{S_1,\ S_2,\ S_3, \ldots,\ S_k,\},$$

where R_i and S_i correspond, respectively, to the symbolic sequences 13100 and 10220, and $k = j/5$ coexist when

$$3 + \Delta + 5k(1+\Delta) < \tau < 2 + 3\Delta + 5k(1+\Delta).$$

The regions in τ-Δ space for which these four spiking patterns are observed are shown in Figs. 4(a)–4(c). Figure 4(d) shows the intersection, $\cap$, of these regions. The fact that

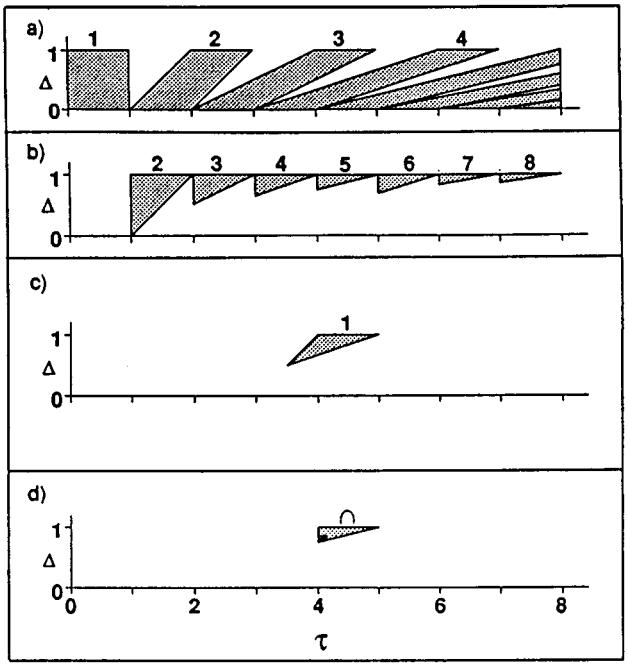

FIG. 4. The regions in τ-Δ parameter space corresponding to the attractors shown in Fig. 2 when $\tau = 4.01$ and $\Delta = 0.89$ [● in (d)]: (a) Fig. 2(a); (b) Fig. 2(b); (c) Figs. 2(c) and 2(d). (d) shows the region in τ-Δ parameter space where all four solutions coexist.

$\cap$ has nonzero measure lies at the basis of the solution multistability of this model. For choices of τ and Δ in $\cap$, all four of the above solutions coexist. Thus it is possible, for example, by introducing a carefully timed inhibitory pulse, to change from one type of pattern to another (Fig. 5).

III. NOISE

We consider the case of Gaussian-distributed white noise [19,20]. Only the timing of the spike is important in our model. Thus it is equivalent to inject noise into either Δ or τ: for convenience we choose to add noise to Δ. Since the interspike interval is $1 + p\Delta$, the lengths of the interspike

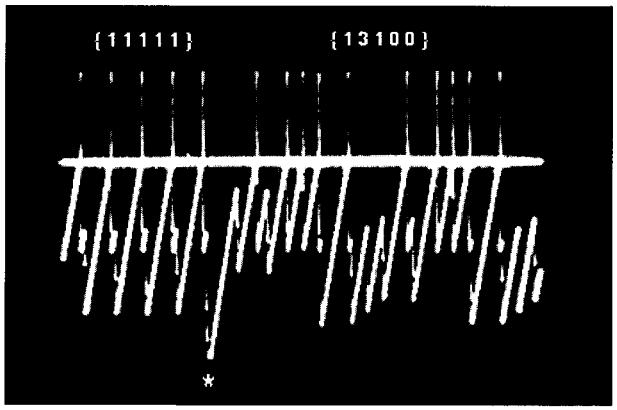

FIG. 5. When $\tau = 4.01$ and $\Delta = 0.89$, a carefully timed inhibitory pulse, indicated by *, induces a transition from one basin of attraction to another. This phenomenon is demonstrated for the electronic circuit described in the Appendix.

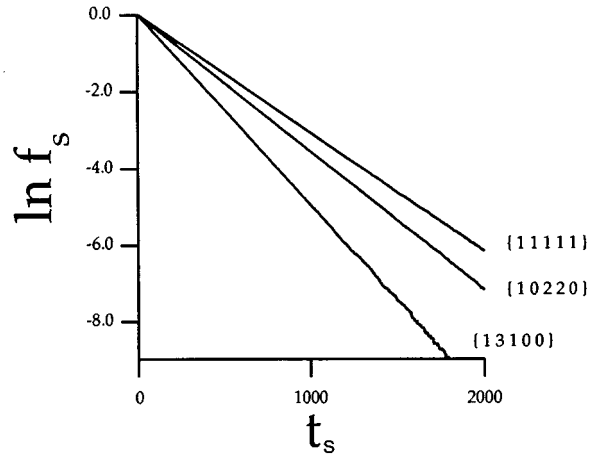

FIG. 6. Plot of the fraction of trajectories f_s remaining in a given basin of attraction at time t_s. The time unit is the standard nondimensionalized time unit used in the model.

intervals will be Gaussian distributed. To illustrate our findings we take $\tau=4.0167$ and $\Delta=0.8918$, which are in the region of overlap of the four attractors described in Sec. II.

To characterize the effects of noise, we measured the dwell times t_s of trajectories in each basin of attraction [21]. The dwell time is defined as the time between when a trajectory first enters a given basin of attraction to the time that it leaves. A trajectory is said to leave a basin of attraction when the number of inhibitory pulses (IP's) in an ISI differs from that expected for the attractor. For example, if we start in the regularly spiking attractor {11111} and see the sequence {112}, we know that the system has just left the attractor. Figure 6 shows that a plot of $\ln f_s$ versus t_s, when f_s, the fraction of trajectories remaining at time t_s, versus t_s is linear. An exponential distribution of t_s is the characteristic distribution observed for the times to cross a threshold in a stochastic [23] or chaotic [24] dynamical system. Thus the observations in Fig. 6 suggest that switches between basins of attraction occur when Δ (or more likely some number of consecutive Δ's) are changed by the appropriate amount.

To illustrate how noise-induced transitions occur between attractors, we discuss the switches from the attractor {11111} to two of the coexisting attractors, {13100} and {10220}. Two steps are involved in a switch between attractors: (1) leaving the first attractor, and (2) entering the second. Once a trajectory leaves the neighborhood of an attractor, it may return eventually to the original attractor, or it may enter a new attractor. Either may occur after an arbitrarily long sequence of transient ISI's. In all cases we observed that the trajectory eventually settles into one of the attractors known to exist in the absence of noise; i.e., no new stable states appear in this system as a consequence of noise [22].

Figure 7 illustrates schematically the most frequent path by which the transition from {11111} to {13100} occurs. For convenience we label with positive subscripts those Δ's that occur after the trajectory leaves the attractor (the onset of the interval with two IP's); negative subscripts refer to those that occur prior to this event. The conditions for the trajectory to leave the attractor by generating an interspike interval with two IP's are

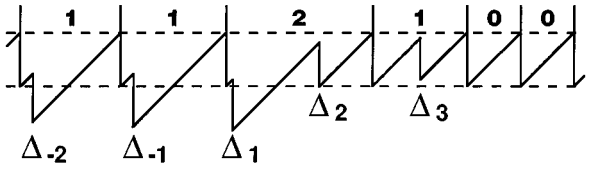

FIG. 7. Most common path by which the transition from {11111} to {13100} occurs. See text for discussion.

$$\xi_{-1}+\xi_1>\tau-2-2\overline{\Delta}, \tag{6}$$

$$\xi_1+\xi_2<\tau-1-2\overline{\Delta}, \tag{7}$$

where $\xi_i=\Delta_i-\overline{\Delta}$ and $\overline{\Delta}$ is the mean value of Δ. The first constraint, Eq. (6), ensures that a second IP falls within the ISI, while the second one, Eq. (7), ensures that the subsequent IP falls in the next ISI. A sequence of three consecutive interspike intervals is required to unambiguously assign the spike train to one of the four coexisting attractors. The condition for the next interspike interval to have exactly 1 IP is

$$\xi_1+\xi_2>\tau-2-2\overline{\Delta} \tag{8}$$

and the condition for the third and fourth interspike intervals to have 0 IP's is

$$\xi_3<\tau-3-\overline{\Delta}. \tag{9}$$

The sequence {100} is unique to the attractor {13100}. Equations (6)–(9) define a volume in four-dimensional space; if the sequence of four Δ's fall within this region a switch occurs between the attractors.

For the transition {11111} to {10220}, numerical simulations indicate that there are two common pathways: 1 1 $\hat{2}$ 0 1 0 2 (path 1) and 1 1 $\hat{2}$ 1 0 1 0 (path 2), where the caret identifies the ISI in which the trajectory leaves the attractor {11111}. By repeating the above calculation, we find that for the first path constraints are required on four Δ's $(\Delta_{-2},\Delta_{-1},\Delta_1,\Delta_2)$; whereas for the second path constraints are required on five Δ's $(\Delta_{-3}, \Delta_{-2}, \Delta_{-1}, \Delta_1, \Delta_2)$.

To illustrate graphically the three most common noise-induced transitions from the attractor {11111} a five-dimensional plot is required. Figure 8 shows cross sections of this space. Only values of ξ's for which transitions were detected are shown. As expected from our discussion, the conditions on the consecutive Δ's that permit switches between attractors appear as thresholds [the solid line is the condition given by Eq. (6)].

The probability P that a given ξ satisfies $a<\xi<b$ is simply

$$P\sim\int_a^b \exp(-u^2/2\sigma)du,$$

where σ is the standard deviation of the Gaussian-distributed white noise. Thus, we can write the total probability for a given transition between two attractors as

$$P=P_1+P_2+P_3+\cdots+P_i, \tag{10}$$

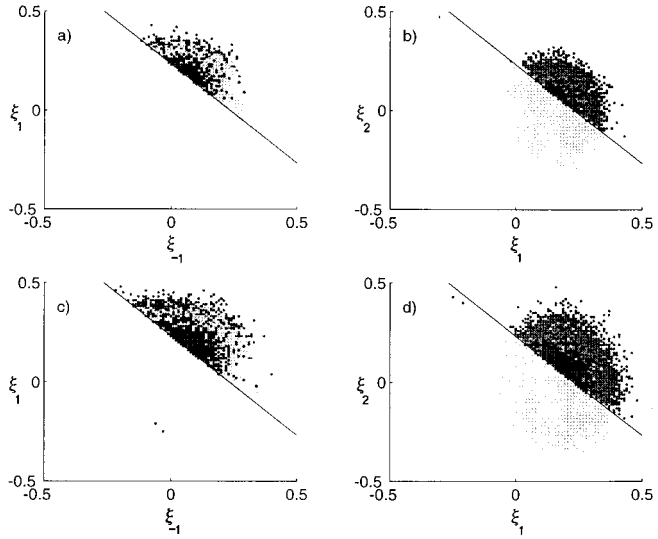

FIG. 8. Cross sections of the space $\xi_{-1},\xi_1,\xi_2,\xi_3,\xi_4$. The values of ξ's for which transitions were detected are scatter plotted. Light gray indicates path 1 for the transition from {11111} to {10220}, black indicates path 2, while dark gray shows the transition from {1111} to {13100}. Each plot is repeated twice at different noise levels to illustrate how increasing noise increases the number of Δ's that fall in the transition regions of the space. Panels (a) and (b) show transitions when $\sigma=0.08$ while for panels (c) and (d), $\sigma=0.10$. Panels (a) and (c) show plots of ξ_1 vs ξ_{-1}. It is clear that Eq. (6) holds for all of the transitions. In panels (b) and (d), ξ_2 is plotted vs ξ_1. Again, we see that for the transition from {11111} to {13100} (8) holds, while for the main transition from {11111} to {10220}, the opposite inequality holds.

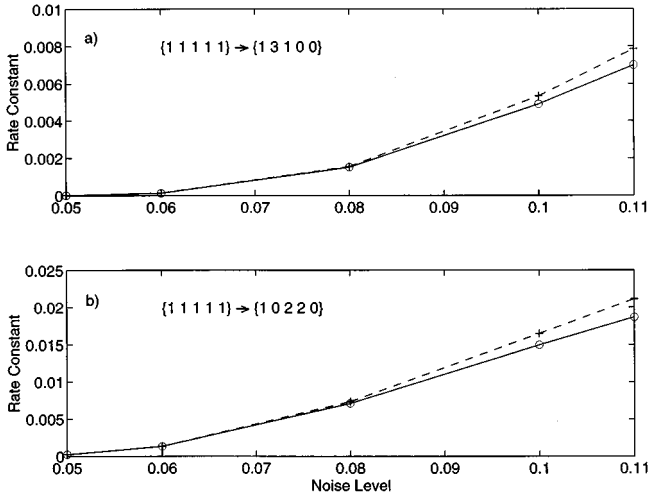

FIG. 9. Plot of the rate constant k for trajectory egress, for each basin of attraction as a function of the noise value (a temperature-like variable). The rate constants are determined by measuring the slope of the plot of $\ln f_s$ vs t_s (Fig. 6). The noise value was measured as the standard deviation of the distribution of Δ. The dashed lines represent the calculated rate constants, while the solid lines reflect the actual measured rate constants. Lines merely connect the data points, which are indicated by their respective markers.

where the P_i are the probabilities that the trajectories escape from the basin of attraction by the ith path. For example, for the transition {11111} to {13100} one path predominates and

$$P\sim P_1=\int_S \exp(-\langle \mathbf{u},\mathbf{u}\rangle/2\sigma)d\mathbf{u}, \tag{11}$$

where $\mathbf{u}$ is a vector and $\langle \mathbf{u},\mathbf{u}\rangle$ denotes the inner product. The integration is performed over the region S described by Eqs. (6)–(9). For the switch from {11111} to {10220} P can be approximated by two terms: one for path 1, the other for path 2.

In general, there are an arbitrarily large number of paths from one attractor to another; however, most of these paths have a negligible probability of occurring for two reasons: constraints on more than five consecutive Δ's and the values of Δ more than three standard deviations from the mean are required. Hence, we can terminate the above sum at an arbitrary amount of precision. Moreover, this is the reason that the third possible transition, which exists for these values of τ,Δ, i.e., {11111} to {00005}, occurs so infrequently.

Figure 9 compares the measured rates [estimated from the slope of $\ln f_s$ versus t_s shown in Fig. 6] s a function of the standard deviation of the injected Gaussian white noise to that calculated from Eq. (10). As can be seen, the measured transition rates agree well with those predicted by Eq. (10).

In principle, the same approach can be used to describe the noise-induced transitions from the other attractors. However, in these cases many more paths for noise-induced transitions arise since not every ISI is equivalent, as they are in {11111}. For instance, when starting in {13100}, there would be five distinct sets of transitions, each corresponding to changing the number of IP's in any one of the standard ISI's. These calculations rapidly become tedious and therefore were not pursued.

IV. DYNAMIC MEMORY STORAGE

In order to obtain a practical assessment of the impact of noise on memory storage by a multistable dynamical system, we constructed an electronic circuit that mimics the integrate-and-fire model discussed in Secs. II and III (Fig. 10). This circuit is fully described in the Appendix. Briefly, neuron E [Fig. 1(a)] is represented by a capacitor that charges linearly. The role of the neuron I is played by a time-delay circuit (bucket brigade device), which introduces an incremental reduction Δ to the capacitor charging voltage at a time τ after the capacitor discharges. In order to put noise on Δ (Sec. III) we added noise to the discharging current source, which normally discharges the capacitor by the exact amount Δ through switch S_2. The noise was generated by a random noise generator (General Radio Company, Model 1390-B) and was first passed through a filter circuit with a time constant of 1 ms.

Figure 11 shows the distribution of interspike intervals for different injected noise levels (measured as $V_{\rm rms}$, the root-mean-square voltage). In all cases the model was initialized to the regular spiking attractor [Fig. 2(a)]. As expected when $V_{\rm rms}=0$, the distribution of ISI is approximated by a single delta function [Fig. 11(a)]. As $V_{\rm rms}$ increases, the distribution of ISI broadens [Figs. 11(b) and 11(c)]. This occurs because the interspike interval is equal to $1+p\Delta$ and noise is injected through Δ. Once $V_{\rm rms}$ becomes large enough, the histogram

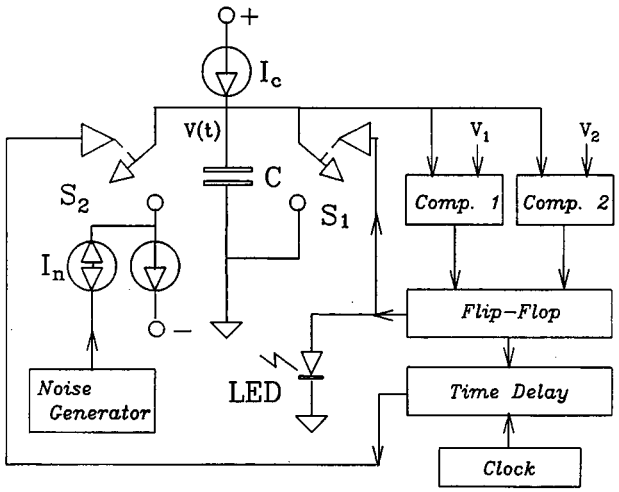

FIG. 10. Schematic diagram of the electronic circuit constructed to mimic a neural recurrent inhibitory feedback loop [shown in Fig. 1(a)] in which the excitatory neuron is modeled by a capacitor. See the Appendix for details.

becomes multimodal [Fig. 11(d)]. These modes appear because once the noise level becomes sufficiently high, switches between basins of attraction frequently occur. The same experiment can be repeated by starting the circuit with a different spiking pattern corresponding to a different attractor. The amplitude of $V_{\rm rms}$ necessary for switches to occur at a noticeable rate depends on the starting attractor. This observation implies that the stability of each attractor to noisy perturbations differs.

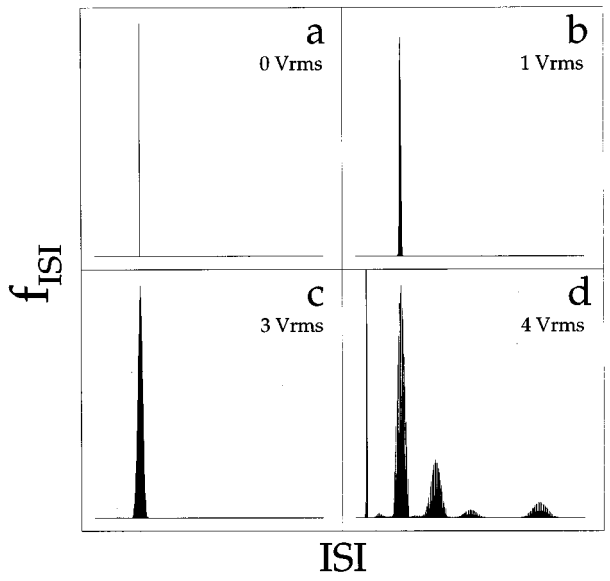

FIG. 11. Interspike interval histograms recorded from the electronic circuit as a function of the $V_{\rm rms}$ of the noise injected into the parameter Δ. The experiment was initiated by using perturbations (Fig. 5) to ensure that the circuit was in the basin of attraction that corresponded to the regular spiking pattern $\{11111\}$. The multimodal histogram in (d) arises when the noise is large enough to cause switches between basins of attraction. When $\tau=4.01$ and $\Delta=0.89$ the possible interspike intervals are $1+p\Delta$, where p equals 0, 1, 2, 3, and 5.

The dwell time t_s discussed in Sec. III corresponds to the time that a memory, represented by a temporal pattern of ISI's, is preserved. A plot of $\ln f_s$ versus t_s is linear with slope k for each of the attractors in this circuit (data not shown). The constant k^{-1} can be interpreted as the average time that a memory persists. When $V_{\rm rms}=4$ V, the average survival times for the attractors in the circuit are $1.5\times10^2\tau$ for $\{11111\}$, $1.25\times10^2\tau$ for $\{10220\}$, $0.75\times10^2\tau$ for $\{13100\}$, and $>2.5\times10^3\tau$ for $\{00005\}$.

In the complete absence of noise, no switching between attractors should occur. However, some switches between attractors occur, albeit rarely, in our circuit in the absence of added noise. The largest source of error in the circuit is the bucket brigade device used to create the delay. The bucket brigade quantizes the delay into 0.14-ms bins. This quantization error acts as a noise source in our circuit and can cause switches between basins of attraction. We estimate that under these conditions the survival times of all of the attractors are $>10^6\tau$.

V. DISCUSSION

Multistability readily arises in control mechanisms with delayed feedback. Since these mechanisms operate in noisy environments, it is likely that noise-induced transitions play a major role in shaping the observed dynamics. The study of noise-induced transitions in multistable dynamical systems is facilitated when the number and properties of the attractors are known. For each choice of τ,Δ it is possible to determine, using the methods we have outlined, the number of coexistent attractors. Although the number of attractors and their basins of attraction can change as a function of τ,Δ, we expect that noise-induced transitions will be qualitatively similar to the example discussed in Sec. III. When $\Delta>1$, the nature of the multistability becomes more complex and will be dealt with in a separate communication.

Two mechanisms exist for noise-induced transitions in multistable dynamical systems [12]. First, a single perturbation can cause a switch between two attractors. Second, the switch between attractors may occur only after a series of perturbations. This latter mechanism is by far the most common one for noise-induced transitions between attractors in systems continuously perturbed by noise such as we study here.

The observations in Figs. 6 and 11 suggest the possibility of characterizing the rates of transition, k, as $k\propto\exp(-E_a/RT)$, where E_a is the height of an effective energy barrier. The temperaturelike variable T is typically proportional to the square of the variance of the noise, i.e., σ^2. It has been shown previously that the rate of noise-induced transition from a chaotic attractor has an exponential dependence on σ^{-2} [21]. In our case, E_a corresponds to the instantaneous energy of the system, and σ, the rms level of the noise on Δ, corresponds to the temperature of the system. Rate constants reflect the probability that the system will make a transition per unit time. In our case, the rate constant is directly proportional to P given in Eq. (10) and depends on σ, not σ^2. The dependence of k on σ is not necessarily exponential. Indeed this dependence may be rather complex through its relation to the erf function. It is quite possible that complex dependencies of k on σ may be a characteristic

feature of noise-induced transitions between multiple limit cycle attractors.

Multistable dynamical systems have potential as memory storage devices [2,6,8]. It is certainly relatively easy to construct multistable electronic circuits (Sec. IV, [7]). However, although for low noise levels the average time that a trajectory remains in a given attractor can be quite long, there is nonetheless a nonzero probability that switches occur between attractors. Thus, noisy multistable dynamical systems are clearly best suited for short-term dynamical memory storage. Our circuit suggests the feasibility of construction of multistate computational devices.

ACKNOWLEDGMENTS

We thank Dr. M. C. Mackey (McGill University), Dr. J. Bélair (Université de Montréal), Dr. A. Longtin (University of Ottawa), and Dr. T. Ohira (Sony Computer Science Laboratory, Tokyo) for useful comments. J.F. was supported by the Lucille P. Markey Charitable Trust and the Women's Council of the Brain Research Foundation. We thank Wayne Garver for technical assistance in constructing the electronic circuit and John Crate for developing the data acquisition system. This work was supported by a grant from the National Institutes of Mental Health and the Brain Research Foundation.

APPENDIX

The schematic diagram of the electronic circuit of the integrate-and-fire model described in Secs. II and III is shown in Fig. 10. Neuron E [Fig. 1(a)] is represented by the capacitor C. This capacitor can be charged with the constant current source I_c and discharged by the two switches S_1 and S_2. Switch S_1 is closed on the leading edge of a pulse from the flip-flop circuit shown. The flip-flop is operated by comparitors 1 and 2, which cause it to change state when the voltage across the capacitor touches either V_1 or V_2, which are fixed at $\frac{1}{3}$ and $\frac{2}{3}$ of the supply voltage, respectively. The comparitors, flip-flop and switch S_1 are actually part of a single chip: the NE555 countertimer chip. In operation, the capacitor charges linearly with time (rate=116 V/s) from V_1 (''resting membrane potential'') until the voltage reaches V_2 (''firing threshold'') at which time S_1 closes and discharges (''neural spike'') the capacitor again to V_1 whereupon the process begins again (in the absence of an inhibitory signal described next). Thus far the circuit operation is identical to a relaxation oscillator with period, $T+(V_2-V_1)/A$ s. Upon discharge by S_1 the flip-flop output is also differentiated and pulse shaped (circuitry not shown) into a sharp spike similar to a neutral firing event.

In order to introduce the delayed inhibitory feedback loop, the flip-flop output is also sent to a time delay circuit. This is a ''bucket brigade'' device: an RD5107 (EG&G Reticon). The bucket brigade is driven by a clock TTL pulse (Hewlett Packard 33120A arbitrary signal generator). The clock frequency determines the time delay: higher frequencies result in smaller time delays. The time-delayed flip-flop pulse then operates switch S_2, which connects to a second constant current source to the negative voltage supply. The magnitude of this current source and the width of the closing pulse on S_2, i.e., the closing time, determine how much charge is removed from C. This results in an incremental reduction in the capacitor voltage by an amount Δ (''inhibitory pulse''). Thus the normal charging cycle of the capacitor is interrupted by the inhibitory signal Δ, which is applied following a time delay τ after every neutral spike. In order to put noise on Δ, as done in the model, we put noise on the discharging current source, which discharges the capacitor though switch S_2, using a random noise generator (General Radio Company, Model 1390-B) whose signal was first passed through a filter circuit with time constant 1.0 ms.

[1] C. C. Canavier, D. A. Baxter, J. W. Clark, and J. H. Byrne, J. Neurophysiol. **69**, 2252 (1993); **72**, 872 (1994).

[2] J. Foss, A. Longtin, B. Mensour, and J. Milton, Phys. Rev. Lett. **76**, 708 (1996).

[3] M. R. Guevara, A. Shrier, and L. Glass, in *Cardiac Electrophysiology: From Cell to Bedside*, edited by D. P. Zipes and J. Jalife (Saunders, Philadelphia, 1990), p. 192; H. A. Lechner, D. A. Baxter, J. W. Clark, and J. H. Byrne, J. Neurophysiol. **75**, 957 (1996).

[4] D. Kleinfeld, F. Raccuia-Behling, and H. J. Cheil, Biophys. J. **57**, 697 (1990).

[5] U. an der Heiden and M. C. Mackey, J. Math. Biol. **16**, 75 (1982).

[6] K. Ikeda and K. Matsumoto, Physica D **29**, 223 (1987).

[7] J. Losson, M. C. Mackey, and A. Longtin, CHAOS **3**, 167 (1993).

[8] T. Aida and P. Davis, IEEE J. Quantum Electron. **28**, 686 (1992).

[9] U. an der Heiden, A. Longtin, M. C. Mackey, J. G. Milton, and R. Sholl, J. Dynam. Diff. Eqs. **2**, 423 (1990); U. an der Heiden and K. Reichard, Z. Angew. Math. Mech. **70**, 621 (1990); S. A. Campbell, J. Bélair, T. Ohira, and J. Milton, CHAOS **5**, 640 (1995); W. Bayer and U. an der Heiden, J. Dynam. Diff. Eqs. (to be published).

[10] J. D. Cowan, in *Statistical Mechanics*, edited by S. A. Ricce, K. F. Fread, and J. C. Light (University of Chicago, Chicago, 1972), p. 181; J. Hertz, A. Krogh, and R. G. Palmer, *Introduction to the Theory of Neural Computation* (Addison-Wesley, New York, 1991); D. Zipser, B. Kehoe, G. Littlewort, and J. Fuster, J. Neurosci. **13**, 3406 (1993).

[11] W. Horsthemke and R. Lefever, *Noise Induced Transitions: Theory, and Applications in Physics, Chemistry and Biology* (Springer-Verlag, New York, 1984); P. Hänggi, P. Talkner, and M. Borkovec, Rev. Mod. Phys. **62**, 251 (1990).

[12] R. Kapral, E. Celarier, P. Mandel, and P. Nordone, SPIE Opt. Chaos **667**, 175 (1986).

[13] S. Fauve and F. Heslot, Phys. Lett. A **97**, 5 (1983); L. Gammaitoni, F. Marchesoni, E. Menichella-Saetta, and S. Santucci, Phys. Rev. Lett. **62**, 349 (1989); A. Longtin, A. Bulsara, and F. Moss, *ibid.* **67**, 656 (1991); F. Moss, D. Pierson, and D.

O'Gorman, Int. J. Bifurc. Chaos **4**, 1383 (1994).

[14] A. Longtin, J. G. Milton, J. E. Bos, and M. C. Mackey, Phys. Rev. A **41**, 6992 (1990); A. Longtin, *ibid.* **44**, 4801 (1991); M. C. Mackey and I. G. Nechaeva, J. Diff. Eqs. **6**, 395 (1994); Phys. Rev. E **52**, 3366 (1995); C. W. Eurich and J. G. Milton, *ibid.* **54**, 6681 (1996).

[15] P. C. Bressloff and J. Stark, Phys. Lett. A **150**, 187 (1990).

[16] J. Lewis, M. Bachoo, C. Polosa, and L. Glass, Brain Res. **517**, 44 (1989); J. Sun, F. Amellal, L. Glass, and J. Billette, J. Theor. Biol. **173**, 79 (1995); J. Lewis, M. Bachoo, L. Glass, and C. Polosa, Phys. Lett. A **125**, 119 (1987).

[17] Since each inhibitory pulse prolongs the period by Δ, it immediately follows that the time between consecutive excitatory spikes is $1+p\Delta$, where p is a non-negative integer. Consider two consecutive inhibitory pulses that occur at times, respectively, t_1 and t_2 in the same interspike interval. Let v_1 be the voltage at t_1. Then $v_1>0$ since two pulses must be at least 1 apart and $0<\Delta<1$. The voltage v_2 is $v_1+(1+p\Delta)-\Delta<1$, where the inequality ensures that the neuron has not fired in the time $[t_1,t_2]$. On rearranging we obtain $0<v_1<(1-p)\Delta$ and hence $p=0$. Since $p=0$, any two pulses in an interval are separated by a positive integer q, and hence $m_v=n_v$.

[18] In a regular spiking pattern, $\{1\}_j$, the inhibitory pulse occurs at the same voltage v_t and time t_t in every interval. Thus $\tau=(j-1)(1+\Delta)+t_t$ (since each spike results in an inhibitory pulse in the jth interspike interval τ later). Solving for t_t and making use of the fact that $0<v_t<1$ we obtain Eq. (5). In a bursting pattern, $\{0,j\}_j$, there are $J-1$ interspike intervals in which no inhibitory pulse occurs and exactly one in which j inhibitory pulses occur. Since the first inhibitory pulse occurs in the jth interspike interval, $\tau>j-1$. For each of the inhibitory pulses in the jth interspike interval, it must be true that the voltage at the time of the ith inhibitory pulse, $v_i<1$, $i=1,\ldots,j$. Thus $\tau-(j-1)+(i-1)(1-\Delta)<1$ for all i. Since $1-\Delta>0$, the most stringent of the inequalities is for the last inhibitory pulse, i.e., the jth one, and hence $\tau<1+\Delta(j-1)$. Thus we obtain Eq. (6). In general, the constraints for any proposed spiking pattern can be obtained by using each of the non-''0'' intervals to obtain conditions on τ. For example, the condition that for each inhibitory pulse, $v_i<1$, $i=1,2,3$, in the ''3'' interspike interval of the more complex spiking pattern, $\{1,3,1,0,0\}_k$, yields Eq. (7). It is easy to verify that the voltages at the times the inhibitory pulse occurs in the ''1'' interspike intervals are less than 1 when Eq. (7) is satisfied.

[19] Gaussian-distributed white noise was created from uniform deviates generated using the Ran1 algorithm that were then put through the Box-Muller transformation to produce normal deviates using algorithms that have been described previously [20].

[20] W. H. Press, B. P. Flannery, S. A. Teukolsky, and W. T. Vetterling, *Numerical Recipes: The Art of Scientific Computing* (Cambridge University Press, New York, 1994).

[21] R. L. Kautz, in *Structure, Coherence and Chaos in Dynamical Systems*, edited by P. L. Peterson and R. D. Parmentier (Manchester University Press, New York, 1989), p. 207.

[22] A. Lasota and M. C. Mackey, *Chaos, Fractals and Noise: Stochastic Aspects of Dynamics* (Springer-Verlag, New York, 1994).

[23] H. A. Kramers, Physica **7**, 284 (1940); O. Legrand and D. Sornette, Physica D **44**, 229 (1990); Phys. Rev. Lett. **66**, 2172 (1991).

[24] M. C. Mackey and J. G. Milton, J. Math. Biol. **28**, 22 (1990); W. Bauer and G. F. Bertsch, Phys. Rev. Lett. **65**, 2213 (1990).